Kinetic and process study for ethanol reforming using a Rh/Pt washcoated monolith catalyst

Amanda Simson [a], Earl Waterman [b], Robert Farrauto [a,b], Marco Castaldi [a,*]

[a] Earth and Environmental Engineering Department, Columbia University in the City of New York, 500 West 120th Street, New York, NY 10027, USA
[b] BASF Catalysts, 25 Middlesex Turnpike, Iselin, NJ 08830, USA

ARTICLE INFO

ABSTRACT

The reforming of pure ethanol was studied over a bi-metallic precious metal (Rh/Pt) catalyst deposited on a ceramic monolith in order to analyze reforming process conditions. High ethanol conversion tests performed at low space velocities ($<20,000$ h^{-1}) confirmed that the catalyst could achieve 100% ethanol conversion to equilibrium concentrations of H_2, CO, CO_2 and CH_4. Low conversion tests at high space velocities ($\geq 50,000$ h^{-1}) were conducted to produce an overall rate expression with an activation energy of 85 kJ mole^{-1}. The reaction was found to have a 1.2 reaction order for ethanol and zero order for water for stoichiometric ethanol and water ratios. In addition, the impact of non-catalytic reactions was studied. The results showed that the catalyst was capable of reforming ethanol as well as the by-products from non-catalytic reactions at 500–700 °C.
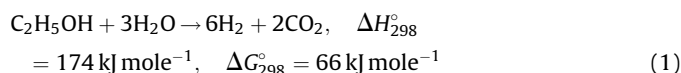
This work is part 1 of a series to develop a process for steam reforming E85 (85% ethanol + 15% gasoline) to generate hydrogen for a fuel cell.

1. Introduction

Ethanol has recently been considered as a potential fuel for generating hydrogen for use in fuel cells because it is produced from renewable sources. As the world begins to focus on more environmentally benign ways to replace fossil fuels, more alcohol and bio-derived fuels will likely be produced. Bio-derived fuels such as ethanol will be used in traditional combustion engine vehicles and will have an associated infrastructure for production and delivery. Ethanol, however, has a low vapor pressure relative to gasoline and therefore it is likely that traditional combustion vehicles will use an ethanol/gasoline blend rather than pure ethanol. Therefore, the next step in examining ethanol steam reforming is to consider the steam reforming of ethanol/gasoline blends (i.e. E85 composed of 85% ethanol and 15% gasoline), since the production and delivery system will be in place for service stations to reform this transportation fuel to hydrogen for fuel cell vehicles. Since gasoline present in E85 contains sulfur we elected to use a non-sulfating carrier in the current study as a baseline for future comparisons with E85.

The steam reforming of pure ethanol produces H_2 according to the following endothermic reaction:

$$C_2H_5OH + 3H_2O \rightarrow 6H_2 + 2CO_2, \quad \Delta H_{298}^\circ$$
$$= 174 \text{ kJ mole}^{-1}, \quad \Delta G_{298}^\circ = 66 \text{ kJ mole}^{-1} \qquad (1)$$

The catalytic steam reforming of ethanol has been reported primarily for Ni-containing catalysts [1–4] and noble metals including Rh [5–11]. These studies have focused on maximizing catalyst activity and hydrogen production and, particularly for the nickel catalysts, have also focused on preventing carbon build-up and deactivation. To date most studies have used powders to investigate fundamental reaction data yet a field process will likely be based on a more structured support. Monolithic ceramic or metal supports washcoated with an active catalyst, allow for low pressure drop and an efficient mechanism for enhanced heat transfer for the endothermic reforming reactions [12]. In order to ensure low pressure drops monolith structures use thin washcoats with high activity catalysts. This study investigates a high activity Rh/Pt catalyst that is less susceptible to coke formation than nickel and can be easily regenerated if coking does occur. This catalyst is also sulfur tolerant which will be important for reforming ethanol/gasoline blends that will contain sulfur.

Recently, bi-metallic catalysts were proposed that would simultaneously promote ethanol steam reforming as well as the forward water gas shift (WGS) reaction to increase H_2 and decrease CO [13]. Several authors have used high water/ethanol ratios to

* Corresponding author.
  E-mail address: mc2352@columbia.edu (M. Castaldi).

enable the WGS reaction to increase hydrogen production. It is well known that Pt is a promoter of the WGS reaction, and Rh/Pt catalysts have been proposed by other authors [13]. The affect of the catalyst carrier has been researched and it has been noted that an alumina carrier promoted the dehydration of ethanol to ethylene and thus promoted coke formation [5,14], however it has also been reported that noble metal catalysts can reform the ethylene to H_2, CO, CO_2 and CH_4 [15]. It has been reported that water concentrations above stoichiometric decrease the likelihood of coke formation [5,16].

Several authors have looked at the kinetics of the steam reforming (SR) reaction over precious metal catalysts. Various research groups calculated activation energies between 1.87 and 23 kJ $mole^{-1}$ over nickel catalysts [17–20]. Vaidya and Rodrigues calculated an overall activation energy of 96 kJ $mole^{-1}$ using a Ru/Al_2O_3 catalyst and found the reaction was first order with respect to ethanol [21]. Sahoo et al. reported an activation energy of 82.7 kJ $mole^{-1}$ for the steam reforming reaction, 43.6 kJ $mole^{-1}$ for the WGS reaction, and 71.3 kJ $mole^{-1}$ for the decomposition reaction on a Co/Al_2O_3 catalyst [22]. Orucu et al. reported an activation energy of 39.3 kJ $mole^{-1}$ for a Pt–Ni/Al_2O_3 [23]. Commonly reported intermediates are acetaldehyde, methane, and ethylene [21,24].

This investigation found that ethanol is very susceptible to thermal decomposition yet few studies have reported the non-catalytic decomposition of ethanol. It was reported by Therdthian-wong et al. that 99% of ethanol decomposed at 650 °C and coke formation was considerable using a stainless steel reactor tube [19]. It was reported by Birot et al. that 18% of the ethanol decomposed at 600 °C on a refractory steel tube [24]. Laosiripojana and Assabumrungrat [3] and Liberatori et al. [2], using a quartz reactor, reported that ethanol decomposed in the absence of a catalyst to acetaldehyde and hydrogen and that the acetaldehyde was further converted to CH_4 and CO in equimolar concentrations. Liberatori noted that this reaction was not affected by the ratio of water/ethanol [2]. Some authors have observed this series of reactions, described by Laosiripojana and Assabumrungrat [3] and Liberatori [2] and also Goula et al. [16] as a non-catalytic reaction and instead attributed it to a catalytic support [4].

The present parametric study provides a baseline for a process to be developed using a precious metal washcoated monolith to reform ethanol for the generation of H_2. It is the first in a series of studies ultimately leading to a process for reforming E85. Initial process conditions have been established for stable performance generating thermodynamic equilibrium mixtures of products. The impact of the non-catalytic decomposition of ethanol on the catalyst activity has also been investigated. Apparent kinetic parameters for the system (reaction orders for the reactants and activation energies) have been determined to provide a basis for further process optimization studies.

2. Experimental

2.1. Catalyst preparation

A commercially available BASF Rh/Pt reforming catalyst (SR10D: BASF # 6218-7C which is available upon request and under secrecy agreement) was used for all catalytic tests. The BASF proprietary catalyst is 4 wt% with a majority being rhodium on a proprietary non-sulfating carrier containing zirconia. An aqueous solution of the catalyst precursor salt was impregnated into the carrier using the incipient wetness method. The impregnated powder was made into a 25% solid aqueous slurry with a pH of 3.4 and ball milled to a particle size less than 10 μ. The catalyst and carrier were deposited on a cordierite ($2MgO–2Al_2O_3–5SiO_2$) monolith with 62 cells cm^{-2} (400 cells $in.^{-2}$) supplied by Corning

Inc. The monolith was coated by dipping into the slurry until the proper loading was achieved. The monolith channels were cleared of excess slurry with a jet of air (air knifing), dried at 120 °C for 2 h and calcined at 500 °C for 4 h. Two catalyst washcoat loadings on the monolith were studied: one with 0.12 g cm^{-3} and one with 0.03 g cm^{-3}. For high conversion tests the catalyst was deposited on a 3.81 cm long, 1.91 cm diameter monolith. For all other conditions the catalyst was tested on a 1.27 cm long, 1.27 cm diameter monolith.

The BET surface area of the finished washcoat was 227 m^2 g^{-1} and the metal dispersion was 31.83% calculated using CO chemisorption at room temperature. The catalyst was reduced in H_2 at 400 °C prior to a pulse CO chemisorption measurement at room temperature. A 1:1 ratio was assumed between CO and Pt and also between CO and Rh. Based on the varying stoichiometry between CO and Rh the dispersion is understood to be an approximate measure.

2.2. Apparatus and procedures

Two reactors were used for testing; one for high conversion, low gas hourly space velocity (GHSV) conditions and another for low conversion, high GHSV conditions. The general reactor schematic for both of these test set-ups is shown in Fig. 1. The difference between the two reactors was the capability of the low conversion reactor to measure H_2O, C_2H_5OH, C_2H_4O species online; the high conversion reactor was not able to do this and thus required a condenser prior to the GC. This ability for the GC to measure room temperature liquid species was important for low conversion tests from which kinetic data was collected. The low conversion tests used an Agilent Micro GC 3000 with inlet heaters that had two molecular sieve columns measuring H_2, N_2, CH_4, and CO and a Plot Q column and an OV-1 column for measuring CO_2, C_2H_4, H_2O, C_2H_5OH, and C_2H_4O. The reactor used for high conversion tests had an Agilent Micro GC with two molecular sieve columns and a PPU column.

Due to undesirable surface reactions of the ethanol with the stainless steel tube wall, the inside of the reactor tube was passivated with Restek Performance Coating's proprietary Silcos-teel coating®. It is a silica based coating that is very adherent to the
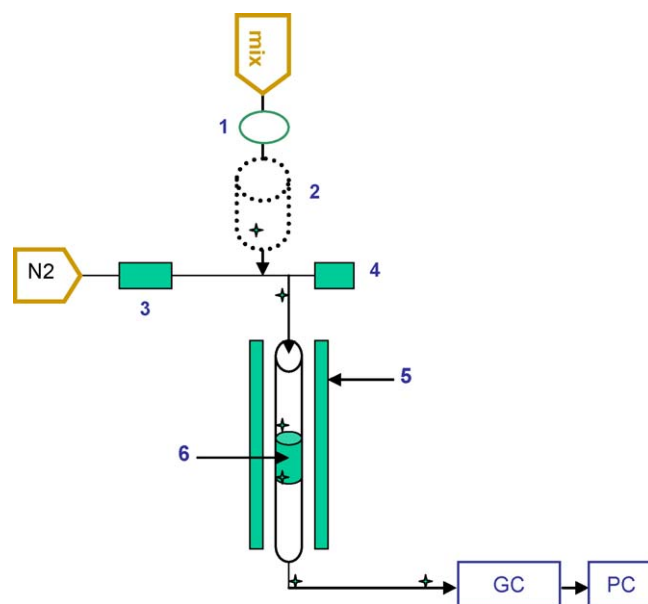

Fig. 1. Schematic of experimental set-up: (1) HPLC pump for feed mix; (2) vaporizer for feed mix; (3) mass flow controls; (4) pressure transducer; (5) furnace; (6) monolith with catalyst washcoat; (*)indicates thermocouple placement.

base metal and is applied to hardware sent to Restek. In both reactor tubes, thermocouples were placed 3.2 mm above and below the monolith as indicated in Fig. 1. All experiments, both blank and catalytic, were done at stoichiometric conditions of 3:1 water/ethanol ratios except when studying reaction orders (as noted in Section 3.1). Nitrogen was used as an internal standard for all test conditions. Heat balance calculations were performed by comparing the measured temperature difference between the inlet and outlet thermocouple with an adiabatic temperature differential based on the enthalpies of measured products at the outlet temperature. The temperature difference calculated by assuming adiabatic operation was within 10% of the measured inlet and outlet temperatures.

2.3. Thermodynamic calculations

Equilibrium values at specified temperatures and pressures were calculated by minimizing the Gibbs free energy using the GASEQ program, which is a graphical user interface to the STANJAN equilibrium program. The product species entered were those which had been identified during experimental tests. The results were determined via Gibbs minimization at experimental outlet temperature and pressure.

3. Results and discussion

3.1. Non-catalytic reactions

It is important to consider the thermal decomposition of ethanol when considering field process conditions. Few authors have reported on non-catalytic reactions and within the reported data on non-catalytic reactions there is a large degree of variance. In this study it was found that thermal reactions did contribute to ethanol conversion or decomposition. It was also found that a surface reaction with stainless steel reactor housings could also occur. Fig. 2 shows ethanol conversion data versus monolith outlet temperature for two tests, one completed in a passivated stainless steel reactor tube and one completed in an unpassivated stainless steel reactor tube. The unpassivated tube walls had a significant effect on overall conversion above 500 °C; at approximately 600 °C the unpassivated reactor contributed an additional 20% ethanol conversion.

Based on product distribution data shown in Table 1, it was clear that the thermal decomposition (in the passivated reactor tube) was a result of the decomposition of ethanol through two
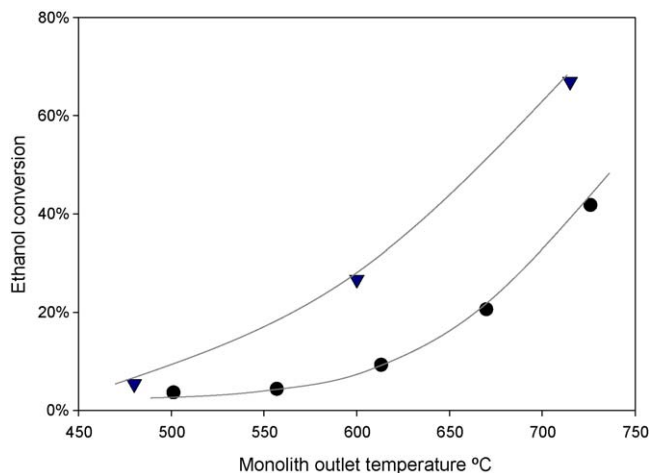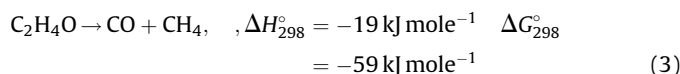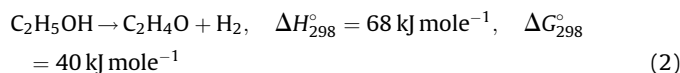
Fig. 2. Non-catalytic reactions for GHSV = 200,000 h^{-1}, 3:1 water/ethanol feed with non-passivated stainless steel reactor tube (▼) and passivated reactor tube (●).

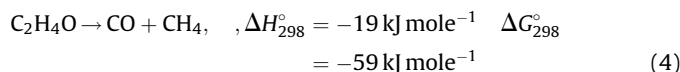**Table 1**
Thermal and surface reactions with blank monolith, GHSV = 200,000 h^{-1}, H$_2$O/C$_2$H$_5$OH = 3:1.

Outlet temperature (°C)	Conversion (%)	Mole product/mole ethanol consumed					
		H$_2$	C$_2$H$_4$O	CO	CO$_2$	CH$_4$	C$_2$H$_4$
Passivated reactor tube with blank monolith (thermal reactions)							
615	8.27	0.95	1.18	0.00	0.00	0.00	0.08
725	43.99	0.82	0.67	0.19	0.00	0.19	0.19
Non-passivated reactor tube with blank monolith (thermal and surface reactions)							
600	28.85	1.00	0.96	0.15	0.00	0.04	0.14
715	72.25	1.24	0.59	0.44	0.01	0.17	0.18

different pathways. One pathway was the decomposition to hydrogen and acetaldehyde followed by the decomposition of acetaldehyde to CH$_4$ and CO as described by Eqs. (2) and (3):
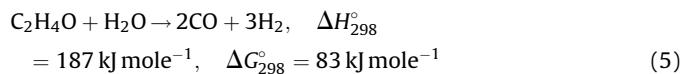
$$C_2H_5OH \rightarrow C_2H_4O + H_2, \quad \Delta H_{298}^\circ = 68\,kJ\,mole^{-1}, \quad \Delta G_{298}^\circ$$
$$= 40\,kJ\,mole^{-1} \tag{2}$$

$$C_2H_4O \rightarrow CO + CH_4, \quad , \Delta H_{298}^\circ = -19\,kJ\,mole^{-1} \quad \Delta G_{298}^\circ$$
$$= -59\,kJ\,mole^{-1} \tag{3}$$

The other decomposition pathway was through the dehydration to ethylene as described by Eq. (4):

$$C_2H_4O \rightarrow CO + CH_4, \quad , \Delta H_{298}^\circ = -19\,kJ\,mole^{-1} \quad \Delta G_{298}^\circ$$
$$= -59\,kJ\,mole^{-1} \tag{4}$$

These results are in agreement with previous work published by Goula et al. [16], Laosiripojana and Assabumrungrat [3] and Liberatori et al. [2] using a quartz tube with no monolith.

Based on these results, the ethanol decomposition attributed to the passivated reactor tube is assumed to be a thermal conversion that should be considered under real process conditions. On the non-passivated tube, higher hydrogen, carbon monoxide, and lower acetaldehyde generation rates indicate that the stainless steel wall is facilitating additional conversion, probably reforming acetaldehyde. There was no change in water concentration for thermal reactions, yet a decrease in water concentration was observed for the reactions on the non-passivated stainless steel surface. The changes in water concentration data and lower acetaldehyde rates in the non-passivated reactor may indicate that the non-passivated stainless steel wall is facilitating a steam reforming reaction according to reaction (5).

$$C_2H_4O + H_2O \rightarrow 2CO + 3H_2, \quad \Delta H_{298}^\circ$$
$$= 187\,kJ\,mole^{-1}, \quad \Delta G_{298}^\circ = 83\,kJ\,mole^{-1} \tag{5}$$

Also, significant coking was found for the tests performed in the non-passivated stainless steel tube. A passivated stainless steel reactor tube was used for all further reported data except as noted in Section 3.4 for high conversion testing. The vaporizer for feedmix section was maintained below 300 °C.

3.2. Role of the catalyst

3.2.1. Catalyst selectivity

In order to study catalyst selectivity washcoat loading was reduced to ensure low conversion conditions. The non-catalytic thermal data, described in Section 3.1 was used as a baseline. Using this technique, it was found that at a washcoat loading of 0.03 g cm^{-3} at a GHSV of 100,000 h^{-1}, or with a higher washcoat loading of 0.12 g cm^{-3} at a GHSV of 200,000 h^{-1} the catalyst had minimal effect on the conversion of ethanol relative to the blank
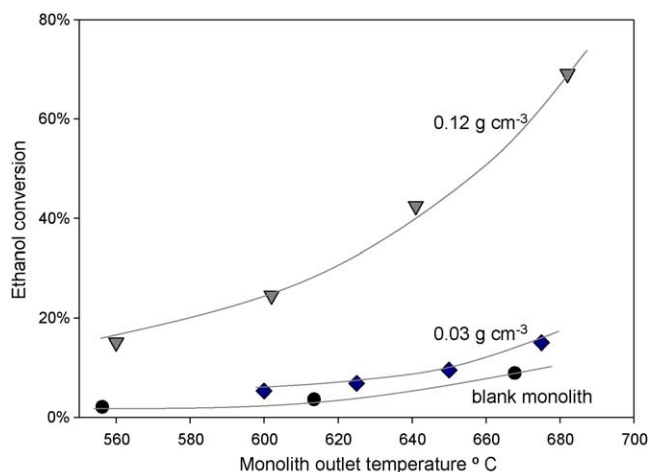
Fig. 3. Various washcoat loadings for GHSV = 100,000 h^{-1}, 3:1 water/ethanol feed with 0.12 g cm^{-3} (▽), 0.03 g cm^{-3} (◆), and the blank monolith (●).

monolith. In Fig. 3, the conversion of ethanol for the catalyst with 0.03 g cm^{-3} and 100,000 h^{-1} showed no increase in conversion relative to the blank monolith. However the catalyst did change hydrogen selectivity and the product distribution, indicating that although the catalyst was not likely contributing to the conversion of ethanol, it was active and converting the thermal decomposition products to H$_2$ and CO as shown in Table 2.

Comparing the catalytic and blank monolith product distributions for the 200,000 h^{-1} condition, shown in Table 2, the ratio of acetaldehyde generated per mole of ethanol consumed is 1.18 for the blank monolith and 0.60 for the catalyst at similar outlet temperatures and similar ethanol conversions. The lower acetaldehyde with the catalyst indicates that the catalyst is reforming the acetaldehyde to products; for the two high temperature conditions the catalyst produces approximately twice as much hydrogen than the blank monolith per mole ethanol consumed. Also, on the catalyst, CO$_2$ was generated between 500 and 700 °C, whereas on the blank monolith no CO$_2$ was generated for any condition. The data indicates that the catalyst is having an effect on the product distribution, without significantly affecting the overall ethanol conversion. For these two conditions, based on the limited increases in catalytic ethanol conversion, and significant differences in acetaldehyde rates, the catalyst is likely reforming the acetaldehyde according to Eq. (5) given in Section 3.1. The dependence of conversion on washcoat loading, seen for the 100,000 h^{-1} condition, may indicate that there is competition for sites between the ethanol and the acetaldehyde. The presence of CO$_2$ in the catalytic product stream, in cases of equal conversion, shows that the catalyst is either producing CO$_2$ from the SR reaction or it is promoting WGS.
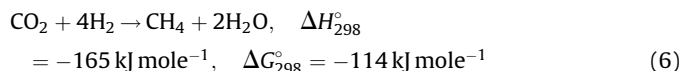
Table 3
Effect of space velocity on catalyst activity, monolith outlet temperature 650 °C, H$_2$O/C$_2$H$_5$OH = 3:1, washcoat loading = 0.12 g cm^{-3}.

GHSV (h^{-1})	Conversion (%)	Mole product/mole ethanol consumed					
		H$_2$	C$_2$H$_4$O	CO	CO$_2$	CH$_4$	C$_2$H$_4$
High loaded catalyst							
50,000	91.58	3.34	0.13	0.67	0.62	0.09	0.04
100,000	40.55	3.50	0.19	0.43	0.79	0.06	0.06
200,000	24.58	1.65	0.51	0.35	0.16	0.12	0.11
Equilibrium values							
	100.00	3.96	0.00	0.97	0.76	0.27	0.00

3.2.2. Influence of gas hourly space velocity

The influence of space velocity on conversion and product distribution was studied. For both washcoat loadings the presence of C$_2$H$_4$ and C$_2$H$_4$O increased with increasing space velocity as shown in Table 3. Previously reported data on rhodium reported these species as reaction intermediates [10,24]. CH$_4$ has also been reported as an intermediate product, however, in the results here, CH$_4$ concentration decreases with increased space velocity for both the high and low loaded catalyst between space velocities of 50,000 and 100,000 h^{-1}. However, between the 100,000 and 200,000 h^{-1} conditions CH$_4$ production increased, possibly indicating that CH$_4$ is both a product and an intermediate species. The methane values were also far from equilibrium values shown in Table 3, even for the point of highest conversion. The results may indicate that CH$_4$ is not an intermediate, as commonly reported, but is formed via CO$_2$ methanation according to reaction (6).

$$CO_2 + 4H_2 \rightarrow CH_4 + 2H_2O, \quad \Delta H_{298}^{\circ}$$
$$= -165 \, kJ \, mole^{-1}, \quad \Delta G_{298}^{\circ} = -114 \, kJ \, mole^{-1} \quad (6)$$

Birot et al. studied a Rh catalyst at similar conditions, but with lower flows (no carrier gas) and higher conversions [24]. Birot et al. found large methane concentrations at low space velocities and attributed it to CO production from the reverse WGS followed by CO methanation [24].

3.3. Overall rate expression calculations

The kinetic evaluation for this system was aligned with determining the apparent kinetics instead of determining intrinsic kinetics. Many researchers have already explored the intrinsic kinetics of PGM catalysts for ethanol reforming [17–23,25,26]. Here we purposely tested the monolith reactor over a range of residence times and initial concentrations to derive a rate expression that can be directly used for monolith reactor design. Unlike typical kinetic studies which maintain conversion of the reactants to less than 5% and limit temperature changes across the

Table 2
Comparison of blank monolith and catalyst, GHSV = 200,000 h^{-1}, H$_2$O/C$_2$H$_5$OH = 3:1, loading for catalyst data = 0.12 g cm^{-3}.

Inlet temperature (°C)	Outlet temperature (°C)	Mole product/mole ethanol consumed						
		Conversion (%)	H$_2$	C$_2$H$_4$O	CO	CO$_2$	CH$_4$	C$_2$H$_4$
Catalyst								
564	600	12.40	1.52	0.60	0.28	0.15	0.07	0.08
618	650	24.58	1.65	0.51	0.35	0.16	0.12	0.19
672	700	47.47	1.63	0.38	0.46	0.13	0.20	0.16
Blank monolith								
583	613	8.27	0.95	1.18	0.00	0.00	0.00	0.08
639	670	19.58	0.81	0.85	0.06	0.00	0.06	0.12
695	726	43.99	0.82	0.67	0.19	0.00	0.19	0.19

catalyst bed to less than 10 °C, here we operated the monolith near adiabatic. This results in a changing concentration and temperature throughout the monolith reactor.

While it is possible to create conditions where the monolith would yield intrinsic kinetics [27], it is also valuable to determine the apparent kinetics that more closely resemble an operating reactor system for ethanol reforming. Therefore, the rate expressions and kinetic parameters reported have temperature and concentration variations along the monolith and incorporate the transport affects associated with monolithic reactor performance. The rate expressions determined here can be coupled to monolith reactor models [28] to extract the concentration and temperature profiles within the monolith reactor. That analysis is outside the scope of the current investigation.

3.3.1. Effective reaction order calculations

As a baseline for an overall process, a global rate expression for the steam reforming of ethanol using the SR10D catalyst was developed. In order to develop an expression to calculate the apparent activation energy, the effective reaction order for water and for ethanol had to be calculated. To calculate an effective reaction order with respect to ethanol, the concentration of ethanol was varied while maintaining a constant water concentration at a monolith outlet temperature of 650 °C. Thus the water/ethanol ratio was changed based on the changes in ethanol concentration. Rates for ethanol and each measured product were calculated based on Eq. (7) where dN_i represents the molar flow rate of species i (i.e. $N_i(in)$–$N_i(out)$) in mole s^{-1} and dW represents the catalyst weight in grams.

$$r_i = \frac{d(N_i)}{W} \tag{7}$$

The apparent reaction rates for ethanol disappearance and acetaldehyde formation followed a similar pattern as shown in Fig. 4, and indicated two separate regimes within the concentrations tested. A separate effective reaction order for ethanol was calculated for each regime.

The initial rate expression was written as Eq. (8):

$$r_{EtOH} = k[C_{EtOH}]^{\alpha}[C_{H_2O}]^{\beta} \tag{8}$$

where α and β represent the effective reaction orders for ethanol and water, k represents the rate coefficient and $[C_{EtOH}]$ and $[C_{H_2O}]$ represent the concentrations of ethanol and water. During the tests total water conversion did not exceed 5% and thus the water term

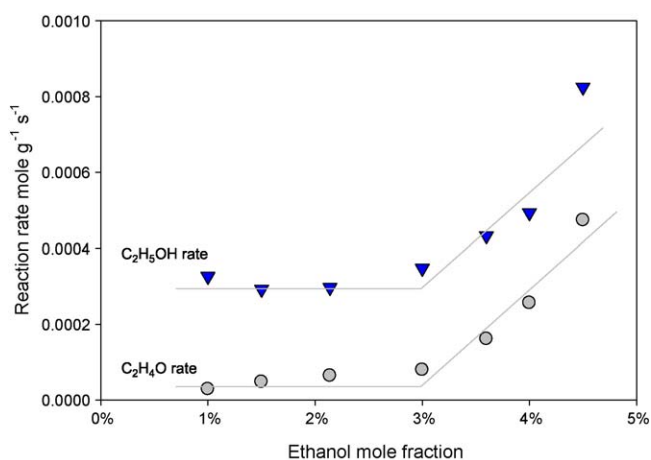**Fig. 4.** Effect of ethanol concentration on production/consumption rates for GHSV = 100,000 h^{-1}, washcoat loading = 0.03 g cm^{-3}, for ethanol (▼) and acetaldehyde (⬤).

Table 4
Influence of ethanol concentration on hydrogen production; monolith outlet temperature = 650 °C, washcoat loading = 0.03 g cm^{-3}. Water concentration is 18% for all cases except the 1.5% ethanol condition for which water concentration was 16%.

Ethanol concentration (%)	Conversion	H$_2$	C$_2$H$_4$O
1.50	37.14	3.22	0.16
2.14	27.00	2.73	0.22
3.00	21.31	2.39	0.23
3.60	28.21	2.60	0.37
4.00	29.09	1.94	0.52
4.50	42.42	1.53	0.57

in Eq. (8) was assumed constant. The reaction rate of ethanol, α, was found according to Eq. (9) which is the natural log of Eq. (8):

$$\ln r_{EtOH} = k + \alpha \ln[C_{EtOH}] \tag{9}$$

where k represents a combination of the k value and the constant water term given in Eq. (8). For the region with ethanol concentrations between 1% and 3% (water/ethanol ratios of 10:1–6:1) an effective reaction order of 0.2 was calculated. For the region with ethanol concentration between 3% and 4.5% (water/ethanol ratios of 6:1–4:1) an effective reaction order of 1.2 was calculated. Several authors reported that the reaction was first order with respect to ethanol [18,21,25] and Orucu et al. noted the reaction order was 1.25 [23]. However, work by Akande et al. on reforming crude ethanol, a 12% ethanol mix [17], and Mathure et al. using pure ethanol [20] noted fractional reaction orders.

During the ethanol concentration variation tests used to determine the effective reaction orders, the mole of hydrogen produced per mole of ethanol consumed were measured and quantified. These results are shown in Table 4. As experimentally reported [4] and determined by thermodynamics, hydrogen selectivity is the highest at the highest water/ethanol ratios. Steam reforming of ethanol, coupled with the WGS reaction, which would produce between 4 and 6 mole of hydrogen, dominates at the highest water/ethanol ratios (lowest ethanol concentrations). At the lowest ethanol concentrations, almost no acetaldehyde is present indicating it is either not a reaction intermediate at high water/ethanol ratio's or instead that it is reformed more rapidly under such conditions; the latter supports the theory that acetaldehyde and ethanol compete for active sites.

3.3.2. Influence of water

Water concentration was varied from 9 to 18% of total feed (water/ethanol ratios of 3:1–7:1) keeping ethanol constant. Similar to the trend shown in Fig. 4 depicting two regions or reaction orders based on changes in ethanol concentration, two separate regimes were also seen based on changes in water concentration. The variance of ethanol conversion rates with water concentration is shown in Fig. 5. At the lowest concentrations of water there was little effect on the rate of ethanol disappearance and the reaction was determined to be zero order, however a negative dependence was found at higher water concentrations. Mas et al. described a similar observation for water dependence [26], a maximum ethanol conversion at water/ethanol ratios of 5:1 with decreasing conversion resulting from increasing water concentrations above this maximum. As shown in Fig. 5, an increase in water concentration increased the hydrogen yield and decreased the presence of acetaldehyde (either by prohibiting its production or facilitating its conversion).

3.3.3. Calculation of apparent activation energy

Conversion versus temperature plots were generated for a 3:1 water/ethanol ratio (15% water, 5% ethanol feed) with the low
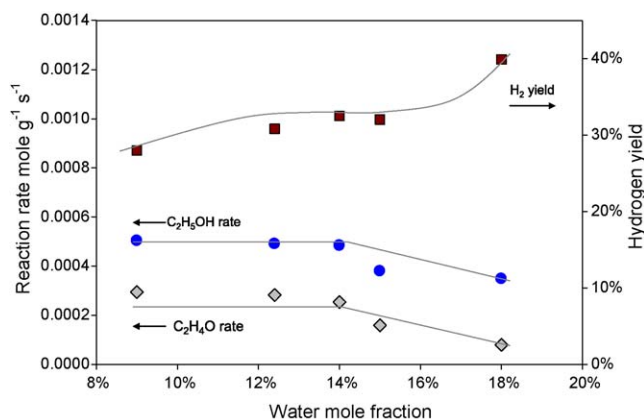
Fig. 5. Effect of water concentration on production/consumption rates for GHSV = 100,000 h^{-1}, washcoat loading = 0.03 g cm^{-3}, for ethanol (●), acetaldehyde (◆), and overall hydrogen yield (■).

Fig. 6. Ethanol conversion values for washcoat loadings of 0.03 g cm^{-3}, 3:1 water/ethanol feed with GHSV = 50,000 h^{-1} (●), GHSV = 75,000 h^{-1}(◆), GHSV = 100,000 h^{-1} (▼).

catalyst loading at outlet temperatures between 600 and 675 °C at GHSV = 50,000, 75,000 and 100,000 h^{-1} in order to generate rate constants for the determination of activation energies. The lower washcoat loading was used to reduce conversion to remain in the kinetic regime. A rate expression was developed by substituting the experimentally determined reaction order from Sections 3.3.1 and 3.3.2 into Eq. (8):

$$\frac{d[C_{EtOH}]}{dt} = -k[C_{EtOH}]^{1.2} \tag{10}$$

Since the experimental conditions were not isothermal and the range of ethanol conversions used were 6–25%, a linear temperature profile was used to represent the temperature change through the monolith from the measured inlet and outlet temperatures. Substituting that into the exponential term for rate coefficient in Eq. (10) yielded the following expression that was integrated for each experimental condition.

$$\int \frac{d[C_{EtOH}]}{[C_{EtOH}]^{1.2}} = A \int e^{-E_{act}^{app}/R(a+bt)} \, dt \tag{11}$$

Here a and b are constants determined from the measured inlet and outlet temperatures. The pre-exponential factor and the apparent activation energy were not considered functions of temperature. Integrating Eq. (11) with respect to time, allowed for a relationship between space velocity (residence time) and ethanol conversion from which to extract A and E_{act}^{app} values by fitting the data. The resulting expression shown in Eq. (12) was integrated numerically (program is available upon request) for each experimental condition:

$$\frac{[C_{EtOH}^{outlet}]^{-0.2} - [C_{EtOH}^{intlet}]^{-0.2}}{-0.2} = A \int_{t_{initial}}^{t_{final}} e^{-E_{act}^{app}/R(a+bt)} \, dt \tag{12}$$

where [C$_{EtOH}$] represents the measured inlet and outlet concentrations of ethanol. The time integral was evaluated using $t_{initial}$ equal to 0.0 and t_{final} equal to the reciprocal of the space velocities in seconds. From the conversion and space velocity data shown in Fig. 6, Eq. (12) was evaluated. Using this procedure the overall activation energy was found to be 85.24 kJ mole^{-1}.

3.4. High conversion test conditions

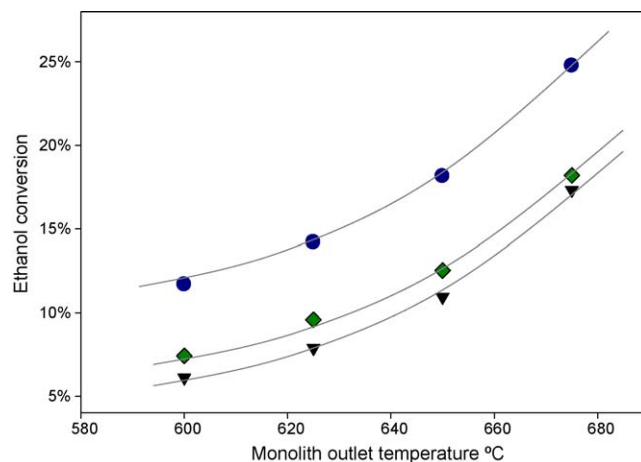A series of high conversion tests were done at low space velocities (<20,000 h^{-1}) and high washcoat loadings (0.12 g cm^{-3}).
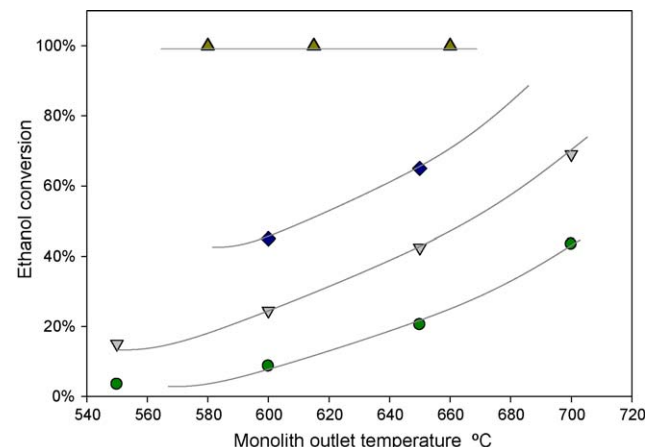

Fig. 7. Ethanol conversion as a function of space velocity for washcoat loading = 0.12 g cm^{-3} for GHSV = 16,000 h^{-1} (▲), GHSV = 50,000 h^{-1} (◆), GHSV = 100,000 h^{-1} (▽), GHSV = 200,000 h^{-1} (●).

Fig. 7 shows results for GHSV = 16,900 h^{-1} versus monolith outlet temperature; this test is plotted with the same catalyst loading as for the higher space velocity conditions detailed in Table 3. For the 16,900 h^{-1} condition a carbon balance indicated 100% of the ethanol
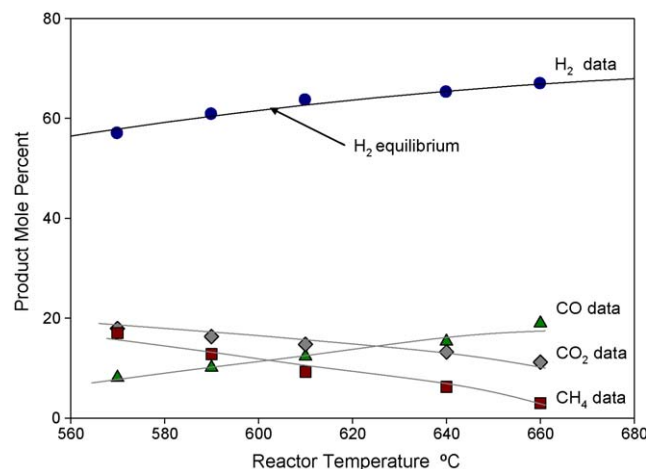

Fig. 8. Product concentrations for GHSV = 16,900 h^{-1}, 3:1 water/ethanol feed with washcoat loading = 0.12 g cm^{-3} of H$_2$ (●), CO (▲), CO$_2$ (◆) and CH$_4$ (■).

was converted to product. This conversion can be attributed to a combination of the thermal, surface, and catalytic reactions based on the discussion in Section 3.1. It was found that in the presence of a catalyst, by-products created based on thermal or surface reactions as described in the previous section, were converted to only H_2, CO, CO_2 and CH_4 as shown in Fig. 8 and H_2 equilibrium values were reached.

4. Conclusions

A Rh/Pt catalyst with a non-sulfating carrier on a monolith converted 100% of the ethanol to H_2, CO, CO_2 and CH_4 essentially achieving equilibrium at stoichiometric conditions and gas hourly space velocity less than 20,000 h^{-1}. The catalyst was able to selectively convert the by-products of non-catalytic reactions to equilibrium product distributions. Both the catalytic and non-catalytic reactions produced intermediates and by-products such as C_2H_4, C_2H_4O. Additionally, a condition was found where the catalyst changes the product distribution relative to the blank non-catalytic reaction but without significantly impacting ethanol conversion. Results at this condition indicate that the ethanol and acetaldehyde may compete for active sites with acetaldehyde being preferentially adsorbed. An overall rate expression was developed with an activation energy of 85 kJ mole^{-1}. The reaction order for ethanol was found to be 1.2, for water/ethanol ratios near stoichiometric. At higher water/ethanol ratios the reaction showed little dependence on ethanol, and the calculated reaction order for this region was approximately 0.2. Changes in water concentration for near stoichiometric ratios of water/ethanol did not affect ethanol conversion but did significantly enhance hydrogen yield likely due to the water gas shift reaction. Additionally, the methanation reaction was suggested as a cause for hydrogen disappearance and methane gains at the lowest space velocities, this could be an important area for study when considering the optimum residence time.

References

[1] A.N. Fatsikostas, X.E. Verykios, J. Catal. 225 (2004) 439.
[2] J. Liberatori, R. Ribeiro, D. Zanchet, F. Noronha, J. Bueno, Appl. Catal. A 327 (2007) 197–204.
[3] N. Laosiripojana, S. Assabumrungrat, Appl. Catal. B 66 (2006) 29–39.
[4] P. Biswas, D. Kunzru, Chem. Eng. J. 136 (2008) 41–49.
[5] D.K. Liguras, D.I. Kondarides, X.E. Verykios, Appl. Catal. B 43 (2003) 345.
[6] H. Idriss, Plat Met. Rev. 48 (2004) 105–115.
[7] S. Cavallaro, Energy Fuels 14 (2000) 1195–1199.
[8] T. Montini, L. De Rogatis, V. Gombac, P. Fornasiero, M. Graziani, Appl. Catal. B 71 (2007) 125.
[9] P. Sheng, W. Chiu, A. Yee, S. Morrison, H. Idriss, Catal. Today 129 (2007) 313–321.
[10] H.S. Roh, Y. Wang, D.L. King, A. Platon, Y.H. Chin, Catal. Lett. 108 (2006) 15.
[11] F. Aupretre, C. Descorme, D. Duprez, Top. Catal. 30 (31) (2004) 487–491.
[12] R. Farrauto, Y. Liu, W. Ruettinger, O. Ilinich, L. Shore, T. Giroux, Catal. Rev. 49 (2007) 141.
[13] M. Ni, D. Leung, M. Leung, Int. J. Hydrogen Energy 32 (2007) 3238–3247.
[14] S. Cavallaro, Energy Fuel 14 (2000) 1195.
[15] J.P. Breen, R. Burch, H.M. Coleman, Appl. Catal. B 39 (2002) 65.
[16] M. Goula, S. Kontou, P. Tsiakras, Appl. Catal. B 49 (2004) 135–144.
[17] A. Akande, A. Aboudheir, R. Idem, A. Dalai A, Int. J. Hydrogen Energy 31 (2006) 1701–1715.
[18] J. Sun, X. Qiu, F. Wu, W. Zhu, Int. J. Hydrogen Energy 30 (2005) 437–445.
[19] A. Therdthianwong, T. Sakulkoakiet, S. Therdthianwong, Sci. Asia 27 (2001) 193–198.
[20] P. Mathure, S. Ganguly, A. Patwardhan, R. Saha, Ind. Eng. Chem. Res. 46 (2007) 8471–8479.
[21] P. Vaidya, A. Rodrigues, Ind. Eng. Chem. Res. 45 (2006) 6614–6618.
[22] D. Sahoo, S. Vajpai, S. Patel, K. Pant, Chem. Eng. J. 125 (2007) 139–147.
[23] E. Orucu, F. Gokaliler, A. Aksoylu, Z. Onsan, Catal. Lett. 120 (2008) 198–203.
[24] A. Birot, F. Epron, C. Descorme, D. Duprez, Appl. Catal. B 79 (2008) 17–25.
[25] L. Arteaga, L. Peralta, V. Kafarov, Y. Casas, E. Gonzales, Chem. Eng. J. 136 (2008) 256–266.
[26] V. Mas, M. Dieuzeide, M. Jobbagy, G. Baronetti, N. Amadeo, M. Laborde, Catal. Today 133 (135) (2008) 319–323.
[27] M. Lyubovsky, L. Smith, M. Castaldi, H. Karim, B. Nentwick, S. Etemad, R. LaPierre, W. Pfefferle, Catal. Today 83 (2003) 71–84.
[28] M. Castaldi, R. LaPierre, M. Lyubovski, W. Pfefferle, S. Roychoudhury, Catal. Today 99 (2005) 339–346.